N-doped TiO2 nanotubes synthesized by atomic layer deposition for acetaminophen degradation

Syreina Sayegh, Mahmoud Abid, Fida Tanos, Geoffroy Lesage, François Zaviska, Eddy Petit, Igor Iatsunskyi, Roman Viter, Emerson Coy, Victoriia Fedorenko, et al.

HAL Id: hal-04102383
https://hal.umontpellier.fr/hal-04102383v1

Submitted on 5 Oct 2023

N-doped TiO₂ nanotubes synthesized by atomic layer deposition for acetaminophen degradation

Syreina Sayegh[1,2], Mahmoud Abid[1], Fida Tanos[1,2], Marc Cretin[1], Geoffroy Lesage[1], François Zaviska[1], Eddy Petit[1], Bruno Navarra[1], Igor Iatsunskyi [3], Emerson Coy[3], Roman Viter[4,5], Victoriia Fedorenko[4], Arunas Ramanavicius[6], Antonio Razzouk[2] , Juliette Stephan[2] and Mikhael Bechelany[1]*

1   Institut Européen des Membranes, IEM UMR 5635, Univ Montpellier, CNRS, ENSCM Place Eugène Bataillon, 34095 Montpellier cedex 5, France.

2   Laboratoire d'Analyses Chimiques, LAC – Lebanese University, Faculty of Sciences, Jdeidet 90656, Lebanon

3   NanoBioMedical Centre, Adam Mickiewicz University, Wszechnicy Piastowskiej 3, 61-614 Poznan, Poland

4   Institut of Atomic Physics and Spectroscopy, University of Latvia, Rainis Blvd., LV-1586, Riga, Latvia

5   Center for Collective Use of Scientific Equipment, Sumy State University, 31, Sanatornaya st., 40018 Sumy, Ukraine

6   Department of Physical Chemistry, Faculty of Chemistry and Geosciences, Institute of Chemistry, Vilnius University, Vilnius, Lithuania
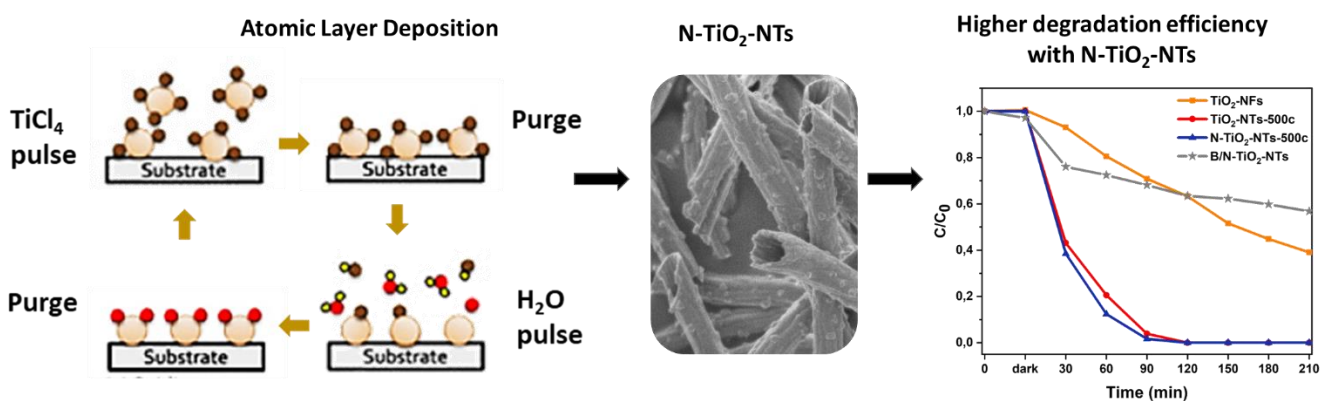
*Corresponding author: _mikhael.bechelany@umontpellier.fr_

ABSTRACT

Titanium dioxide (TiO_2) is widely used in photocatalysis applications for wastewater treatment. Investigations demonstrated that titanium dioxide structure strongly contributes to increase micropollutant degradation efficiency. Indeed, pollutant degradation rates are enhanced when using photocatalysts with highly ordered structures and high specific surface area, such as TiO_2 nanotubes (NTs) synthesized by atomic layer deposition (ALD). Here, TiO_2 NTs, fabricated by ALD followed by nitrogen doping via thermal treatment, were compared with TiO_2 nanofibers (NFs), prepared by electrospinning. Their morphology and structure were investigated by scanning and transmission electron microscopy, X-ray diffraction, and X-ray photoelectron spectroscopy. Photoluminescence measurements showed that TiO_2 NT photoluminescence intensity was lower than that of TiO_2 NFs, due to lower electron-hole pair recombination, and consequently their degradation efficiency was higher. As the surface to volume ratio was higher in TiO_2 NTs than NFs, the rate of non-radiative surface recombination also was higher in TiO_2 NTs. Comparison of their performance for photocatalytic degradation of acetaminophen showed higher degradation activity with TiO_2 NTs than TiO_2 NFs. TiO_2 NT doping with nitrogen (N-TiO_2 NTs) further enhanced their photocatalytic activity that was 5 times higher than that of TiO_2 NFs (degradation rates: 0.05 and 0.01 mg.L^{-1}.min^{-1}, respectively). The N-TiO_2 NT photocatalyst was stable after four cycles of acetaminophen degradation. Acute toxicity assays confirmed the release of harmful by-products during the first hours of acetaminophen degradation, but toxicity strongly decreased after 5 hours.

Keywords: TiO_2 nanotubes; N-doped TiO_2; atomic layer deposition; photocatalysis; acetaminophen

Graphical abstract

Atomic Layer Deposition

TiCl$_4$ pulse → Substrate → Substrate → Purge

Purge ← Substrate ← Substrate ← H$_2$O pulse

N-TiO$_2$-NTs

Higher degradation efficiency with N-TiO$_2$-NTs

- TiO$_2$-NFs
- TiO$_2$-NTs-500c
- N-TiO$_2$-NTs-500c
- B/N-TiO$_2$-NTs

C/C$_0$ vs Time (min)

Highlights

- TiO$_2$ nanotubes (NTs) were fabricated by atomic layer deposition on polyacrylonitrile nanofibers

- The as-prepared samples efficiently degraded acetaminophen upon visible light exposure

- The photocatalytic efficiency of TiO$_2$ NTs was 3 times higher than that of TiO$_2$ nanofibers after 90 minutes of visible light irradiation

- Nitrogen doping further improved TiO$_2$ NT degradation efficiency by increasing the separation time of the photogenerated charge carriers

- N-TiO$_2$ NTs displayed the lowest charge transfer resistance and the largest electroactive surface area

1. Introduction

The pressing increase in clean water demand has led researchers to focus on developing new technologies for water treatment because the conventional systems cannot efficiently degrade micropollutants (e.g. drugs, pesticides, personal care products, dyes) and eliminate microorganisms[1,2] that can resist to the conventional methods and then contaminate drinking water[3,4]. Although these contaminants are usually present at very low concentrations, they can harm human health and other living organisms[5,6]. For instance, acetaminophen (ACT) is a pharmaceutical product used as painkiller that have been detected in the range of ppm to ppt and has significant negative impacts to the aquatic and ecological systems[7].

The main challenge is the development of new removal techniques that are cheap and require less energy consumption. Advanced oxidation processes (AOP), particularly photocatalysis, are good candidates at the place or in combination with conventional techniques[8–10]. Photocatalysis is a green technology in which, pollutants under visible light irradiation are degraded to CO_2, H_2O, and in some cases small non-toxic molecules , as final degradation products.[11,12] In this system, upon irradiation, the semiconductor is activated by photon energy that is equal to or higher than its bandgap energy. This leads to the formation of electron-hole pairs between the conduction and valence bands that will then generate radicals implicated in the pollutant mineralization[13,14].

Titanium dioxide (TiO_2) is among the most used semiconductors. TiO_2 is not expensive and displays good chemical and thermal stability and low toxicity[15–18], but its wide bandgap and fast electron-hole pair recombination limit its use under visible light[19–21]. Previous studies on the development of materials and technologies with higher degradation efficiency for water treatment indicate that the catalyst structure and morphology strongly contribute to its catalytic activity under visible light. [22–24] In agreement, TiO_2 photocatalytic activity is influenced by its morphology, crystallinity, surface, and textural properties. Many groups have tried to tailor TiO_2 morphology to increase its photocatalytic performance[25–28]. For instance, 0D, 1D, 2D and 3D TiO_2-based materials have been fabricated using various techniques[29–33]. One-dimensional (1D) materials, such as 1D TiO_2 nanofibers (NFs), nanorods, nanotubes (NTs),

nanowhiskers and nanowires[34–36], are particularly interesting due to their higher light absorption and slower recombination rates, leading to better photocatalytic activity[37–39]. Among these structures, tubular nanostructured TiO_2 is a versatile material for photocatalysis and photoelectrolysis[40–42]. Many preparation techniques have been tested for fabricating such 1D nanostructures (e.g. hydrothermal synthesis, template synthesis, anodization, electrospinning and atomic layer deposition, ALD) [43–46]. ALD is a thin film deposition technique based on gas-phase precursors for the deposition of thin-film layers with thickness control at the Ångstrom level[47–49]. ALD has been often combined with electrospinning for the deposition of the desired materials on polymeric fibers that are used as substrate[50–53]. Upon removal of the polymeric core by thermal treatment after the ALD cycles, a tubular structure is formed[54]. McClure *et al.* described TiO_2 deposition on polymeric nanofibers by ALD, and then compared the precursor effect on the film coating. They found that the precursor choice influenced the final structure of TiO_2 NTs[55]. Su *et al.* reported the fabrication of TiO_2 NTs by ALD using titanium chloride and H_2O as precursors and assessed the doping effect on NT photocatalytic and photoelectrochemical performance[56]. In addition, the number of ALD cycles and the deposition temperature may affect the material crystalline structure[45].

As TiO_2 catalysts are often not stable and not much active under visible light irradiation, improving TiO_2 morphology might positively influence the photocatalytic behavior compared with unmodified TiO_2 (commercial Degussa p25)[57]. Several methods have been described to extend the semiconductor photo-response to the visible light region, such as doping TiO_2 with metals and non-metals and coupling with other semiconductors[58–60]. Doping with non-metals (e.g. carbon, sulfur, phosphorus, nitrogen[61–65]) reduces the recombination of photogenerated electron-hole pairs in TiO_2. Several non-metal dopants were mentioned in the literature such as carbon (C), sulfur (S), phosphorus (P) and nitrogen (N)[61–65]. N-doping is the most studied[66] and allows shifting the TiO_2 band into the visible light range[67]. Asahi *et al.* found that N-doping extends TiO_2 optical absorbance towards the visible light region[68]. Moreover, the presence of non-metals in TiO_2 generally increases the specific surface area and the anatase phase percentage, while limiting the crystallite size growth[69]. Huang *et al.* fabricated N-doped TiO_2 (N-TiO_2) by hydrothermal synthesis and calcination under NH_3 atmosphere. They found that N-doping promoted the generation of hydroxyl and superoxide radicals that enhanced the photocatalytic activity[70]. Another study showed that N-doping promotes the formation of

oxygen vacancies that contribute to visible light absorption[59]. These two effects were also observed in hierarchical structures grown by ALD in which N-doping of TiO_2 was obtained by incorporating N atoms on the substrate[71]. Hence, co-doping TiO_2 with nitrogen and boron can enhance both the visible light absorption of TiO_2 and implement an efficient charge recombination regarding the synthesis technique[72].

On the other hand, it was widely reported that the morphologies of 1D structures can influence TiO_2 photocatalytic properties. Interestingly, the photocatalytic activity can be tuned by several parameters such as particle size, specific surface area, porous structure, crystalline phase etc. [19]. Rosales *et al.* compared the photocatalytic activity of different 1D morphologies (NTs, NFs, NWs) on the degradation of methyl orange. The author found that the shape of TiO_2 has a major role in determining their photocatalytic activity[34], herein the importance of comparing different 1D morphologies such as TiO_2 nanofibers and nanotubes for the degradation of organic micropollutant.

Here, we fabricated 1D TiO_2 NTs by ALD for photocatalysis. To the best of our knowledge no previous reports have been published on elaboration of TiO_2 nanotubes by Atomic Layer Deposition for catalytic activity. Hence 1D TiO_2 NTs have shown a great interest for the degradation of micropollutants when compared to NFs and NWs because of their higher efficiency to absorb light. Variation of the number of ALD cycles confirmed that the photocatalytic efficiency was directly influenced by the NT wall thickness. Moreover, TiO_2 doping with non-metals (nitrogen) further improved the photocatalytic activity by modifying the NT charge transportation, surface area, reflection and absorption. By comparing the catalytic activity of these TiO_2 NTs and of TiO_2 NFs prepared by electrospinning we found that ALD allows the formation of a well-structured nanotubular catalyst with higher degradation efficiency than NFs. More than 98% of acetaminophen was degraded in the presence of N-TiO_2 NTs after 180 min of visible light irradiation. N-TiO_2 NTs recyclability and toxicity tests showed the potential of this catalyst for real applications. We also performed quenching tests to determine the active species responsible for acetaminophen degradation.

2. Experimental

2.1. Materials and chemicals

Titanium(IV) isopropoxide (TTIP, 97%, CAS: 546-68-9), titanium (IV) chloride (TiC$_{l4}$, 99.9%, CAS: 7550-45-0) , polyacrylonitrile (PAN, Mw=150000, CAS: 25014-41-9), polyvinyl pyrrolidone (PVP, Mw=1300000, CAS: 9003-39-8), acetaminophen (≥99%, CAS: 103-90-2), formalin solution (HCHO, CAS: 50-00-0), boron tribromide (BBr$_3$, 99.9%, CAS :10294-33-4), Nafion™ perfluorinated resin solution (CAS: 31175-20-9), potassium chloride (KCl, ≥99%, CAS:), sodium sulfate (Na$_2$SO$_4$, ≥99%, CAS: 7757-82-6), sodium chloride (NaCl, ≥99%, CAS: 7647-14-5, potassium ferricyanide (K$_3$[Fe(CN)$_6$], ≥99%, CAS 13746-66-2), 2-propanol (99.9%, CAS: 67-63-0), p-benzoquinone (C$_6$H$_4$O$_2$, ≥99.5%, CAS:106-51-4), and ethylenediaminetetraacetic acid (EDTA, 99.995%, CAS: 60-00-4) were purchased from Sigma-Aldrich. Tetrahydrofuran (99.9%, CAS: 109-99-9) was bought from Honeywell. Acetic acid (≥96% CAS: 64-19-7) and ethanol (≥99.8% CAS: 64-17-5) were purchased from VWR Chemicals and used as solvents. All chemicals were used without any additional purification. Indium tin oxide (ITO) deposited on quartz was purchased from Präzisions Glas & Optik. Deionized water (>18.2 MΩ), prepared with the Millipore (Milli-Q® Academic) water purification system, was used for all dilutions and reagent preparation. Argon gas, ammonia and nitrogen were from Linde and were used as received.

2.2. Support and catalyst preparation

2.2.1. Synthesis of TiO$_2$ nanofibers and PAN nanofibers by electrospinning

For TiO$_2$ NF fabrication, a mix of TTIP, PVP, acetic acid and ethanol was stirred for 2h before electrospinning. The solution was loaded into a 22 mL syringe, and the needle was connected to high voltage. The electrospinning conditions were: needle-collector distance of 10cm, tension of 25kV, and solution flow of 1mL.h^{-1}. For the preparation of PAN NFs, 18mL of tetrahydrofuran was mixed with 2 mg of PAN at 60 °C for 24 h and then electrospinned using a previously described home-built electrospinning system[50,51,73]. The collected TiO$_2$ NFs underwent calcination at 750 °C for 4h before utilization. PAN NFs were stabilized at 250 °C for 2h (heating rate of 1 °C.min^{-1}) before ALD.

2.2.2. Deposition of TiO$_2$ nanotubes by atomic layer deposition

Stabilized PAN NFs were used as substrates for TiO_2 deposition at 100°C, using $TiCl_4$ and H_2O as precursors in a home-built ALD device. After ALD deposition, we removed the PAN upon annealing under air at high temperatures allowing to transform into nanotubes structures.

The typical ALD cycle consisted of 0.2 s $TiCl_4$ pulse, followed by 10 s exposure and 60 s purge. Then, the H_2O valve was opened for 2 s, followed by 10 s exposure and 60 s purge with argon gas. The line connected to the reactor was heated at 100°C to avoid condensation. The number of ALD cycles varied between 500 and 1000 to vary TiO_2 shell thickness. After TiO_2 deposition, PAN-TiO_2 NTs were heated at 750°C for 4h with a heating rate of 1 °C/min under air before use.

2.3.   Nitrogen-doped and boron/nitrogen-co-doped TiO_2 NTs

After 500 ALD cycles, PAN-TiO_2 NTs were exposed to nitrogen at 750°C for 15 min and the samples were denoted (N-TiO_2 NTs) hereafter. For boron/nitrogen co-doped TiO_2 NTs (B/N-TiO_2 NTs), BN was deposited following a previously described method and five ALD cycles were used in this case[73].

2.4.   Characterization of the synthesized nanocomposites

The NT and NF morphology was analyzed by scanning electron microscopy (SEM Hitachi S4800, JAPAN). Samples were placed on aluminum stubs and were sputter-coated with platinum/palladium using a Polaron SC7620 Mini Sputter Coater. X-ray diffraction (XRD) analyses were carried out using a PanAlytical X'pert system with Cu K α radiation (λ = 0.15406 nm). The diffraction patterns were measured between 10 and 80° with a step size of 0.0167°. The tubular morphology NTs was confirmed by transmission electron microscopy (TEM) using the JEOL 2200FS (200 kV) and JEOL ARM-200F (200kV) microscopes. For TEM analysis, samples were dispersed in ethanol, and a drop of the suspension was dried on a carbon support film that covered a standard copper grid. The samples' chemical composition and bandgap were determined by X-ray photoelectron spectroscopy (XPS) measurements, with an Escalab 250 apparatus, and by UV–Visible spectrophotometry (Jasco model V570; equipped with a diffuse reflectance attachment (Shimadzu IRS-2200)), respectively. Optical absorbance was measured by recording the photoluminescence spectra with an optical fiber spectrometer (Ocean Optics

usb2000), equipped with excitation wavelength of 266 nm anda nitrogen Nd:YAG laser of 9mW.

2.5.   Electrochemical measurements

Electrochemical impedance spectroscopy (EIS) and electrochemical active surface (EAS) characterization carried out by cyclic voltammetry (CV) were performed in a three-electrode cell system connected to a Solartron SI 1287 galvanostatic-potentiostat. A halogen lamp (150 w), placed at a distance of 10 cm from the electrode surface, was used as the light source. Platinum wire and Ag/AgCl were the counter and reference electrode, respectively. The working electrode (2x2.5cm) was a suspension of 5 mg photocatalyst, 1 mL isopropanol, and 40 µL Nafion® aqueous solution. After 30 min in an ultrasonic cleaner, this suspension was dropped on the ITO glass, to obtain the working electrode after isopropanol evaporation. For EIS measurements, the three electrodes were immersed in a Na_2SO_4 solution (0.1 $mol.L^{-1}$) considered as the electrolyte. For EAS analysis, 10 mM $K_3[Fe(CN)_6]$ and 1.0 M KCl were used as electrolytes. The samples' electroactive surface area was estimated by CV performed in a voltage range of -0.4 to 0.8 V vs reference at scan rate of 20 $mV.s^{-1}$. The EAS was calculated using the Randles–Sevcik equation:

$$\mathbf{Ip = 2.69 \times 10^5 \times AD^{1/2} \times n^{3/2} \times Cv^{1/2}} \tag{1}$$

where Ip is the maximum current (A), n is the number of transferred electrons (n = 1), A is the electrode area (cm^2), D is the diffusion coefficient of $[Fe(CN)_6]^{3-}$ (7.60×10^{-6} $cm^2.s^{-1}$), C is the concentration of $[Fe(CN)_6]^{3-}$ (1×10^{-5} $mol.cm^{-3}$), and v is the scan rate (0.01 $V.s^{-1}$).

2.6.   Acetaminophen degradation

The TiO_2 samples' photocatalytic activity under visible light (linear halogen lamp; 400W, Avide) was tested by quantifying acetaminophen degradation in an aqueous solution. The solution was maintained at 10 cm from the lamp for all experiments. First, TiO_2 NT samples with different wall thicknesses (different ALD cycle number) were compared. Then, the catalytic performances of TiO_2 NTs (500 ALD cycles), TiO_2 NFs, and doped TiO_2 NTs were evaluated.

The photocatalytic degradation experiments were performed in the following conditions: the photocatalyst with an initial concentration of 0.5 g.L^{-1} was added to 250 mL of acetaminophen aqueous solution (5 mg.L^{-1}) in a 600 mL glass reactor put in a water bath at 30°C to minimize the temperature increase in the solution under light irradiation. After stirring in the dark for 30 min to ensure equilibrium adsorption, the solution was exposed to visible light and at different intervals, 2 mL aliquots were collected and filtered with 0.22 µm filters. Acetaminophen degradation was quantified by high-performance liquid chromatography coupled to a Quattro-Micro mass spectrometer with an Electrospray ionization probe (Waters Micromass, Wythenshawe, Manchester, UK) as detector (HPLC-MS). The separation was carried out using a C-18 column (RP18 Column, Nucleoshell). The mobile phase was composed of Buffer A (0.1% formic acid in HPLC-grade water) and Buffer B (0.1% formic acid in HPLC-grade acetonitrile) with a 97:3 (A:B) ratio. The flow rate was set at 0.25 mL min^{-1} and the run time was 3 min.

The recyclability of the catalyst with the highest degradation efficiency was further investigated for 5 cycles of acetaminophen degradation in the same conditions.

The degradation efficiency (D(%)), was calculated according to equation (2):

$$\mathbf{D(\%) = [(C_0 - C)/C_0] \times 100} \tag{2}$$

where C_0 and C are the initial and final acetaminophen concentrations after the test, respectively.

2.7. Photocatalytic kinetic model

TiO$_2$ degradation kinetics is usually described using the Langmuir–Hinshelwood model[74,75]. When the pollutant concentration is low, a pseudo-first-order kinetics is applied[76], as described in Equation (3):

$$\mathbf{\ln(C_0/C) = kt} \tag{3}$$

where C_0 (mg/L) is the initial pollutant concentration, C is the pollutant concentration at time t (min), and k (min^{-1}) is the pseudo-first-order rate constant.

2.8. Eco-toxicity assays

During acetaminophen degradation many by-products may be formed [77]. To assess their toxicity, inhibition of *Vibrio fischeri* bioluminescence was monitored using a Microtox® Model 500 Analyzer (Modern Water Inc.; United Kingdom) as previously described[69].

2.9.   Quenching tests

Scavenger tests were performed to determine the main active species responsible for acetaminophen degradation. Benzoquinone, isopropanol and EDTA were added to the solution at a concentration of 10 mM before exposure to visible light (same conditions as for the degradation experiments). Aliquot were collected at different intervals, and acetaminophen concentration was measured by HPLC-MS as described in 5.6.

3.   Results and Discussion

3.1.   Morphological characterization

The morphology of all prepared materials (calcinated TiO_2 NFs after electrospinning and TiO_2 deposited on PAN NFs by ALD) was verified by scanning electron microscopy (SEM). Before the analysis, TiO_2 was deposited on PAN nanofibers substrate by ALD and TiO_2 nanofibers elaborated by electrospinning were subject to thermal treatment at 750°C under air for 4h. A well nanotubular structure was observed after ALD deposition with a TiO_2 pulse time of 0.2 s, but not with shorter pulse times (Erreur ! Source du renvoi introuvable.). In addition, it was reported elsewhere that more than 200 ALD cycles are necessary to obtain well-structured NTs[78]. Moreover, **Figure 1a** shows TiO_2 nanotubular morphology of several microns in length after removal of the PAN substrate. This indicates that PAN NFs were an efficient 'template' for TiO_2 NT synthesis. TiO_2 NTs with an inner diameter of approximatively 400 nm and high surface roughness were obtained after 500 ALD cycles (**Figure 1b**). SEM confirmed the nanofibrous structure of TiO_2 NFs (**Figure 1(c)**). The surface roughness is attributed to the crystalline structure of the nanofibers at 750°C. No clear difference was observed after NT doping (**Figure 1 (d-e)**), confirming the previous findings that N- and B-doping do not change TiO_2 shape[70] and that doping with non-metals could occur in the NT bulk[79].
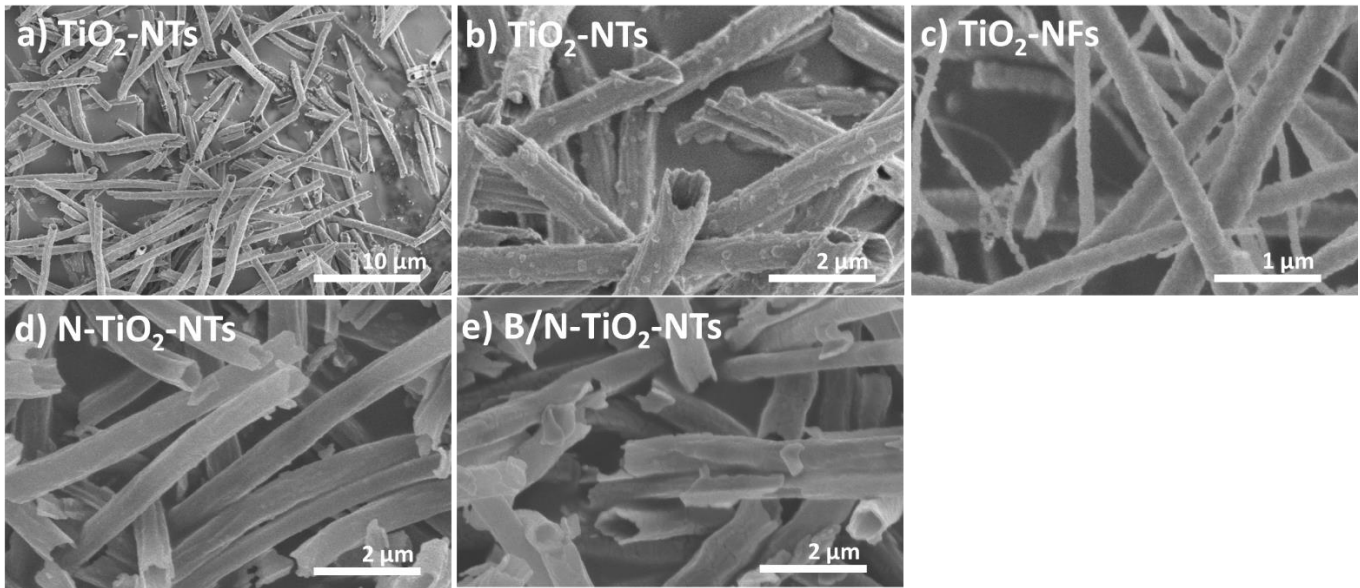
Figure 1. SEM images of (a-b) TiO$_2$NTs, (c) TiO$_2$ NFs, (d) N-TiO$_2$ NTs, and (e) B/N-TiO$_2$ NTs.

TEM images (**Figure 2**) confirmed TiO$_2$ NT nanotubular structure with a nanotube wall thickness of ~60 nm in doped and non-doped samples. After N-doping, TiO$_2$ nanotubular morphology and crystal lattice values (selected area electron diffraction images (SAED)) were not changed. Moreover, elemental mapping (**Figure 2b**) indicated the presence of N, T and O.
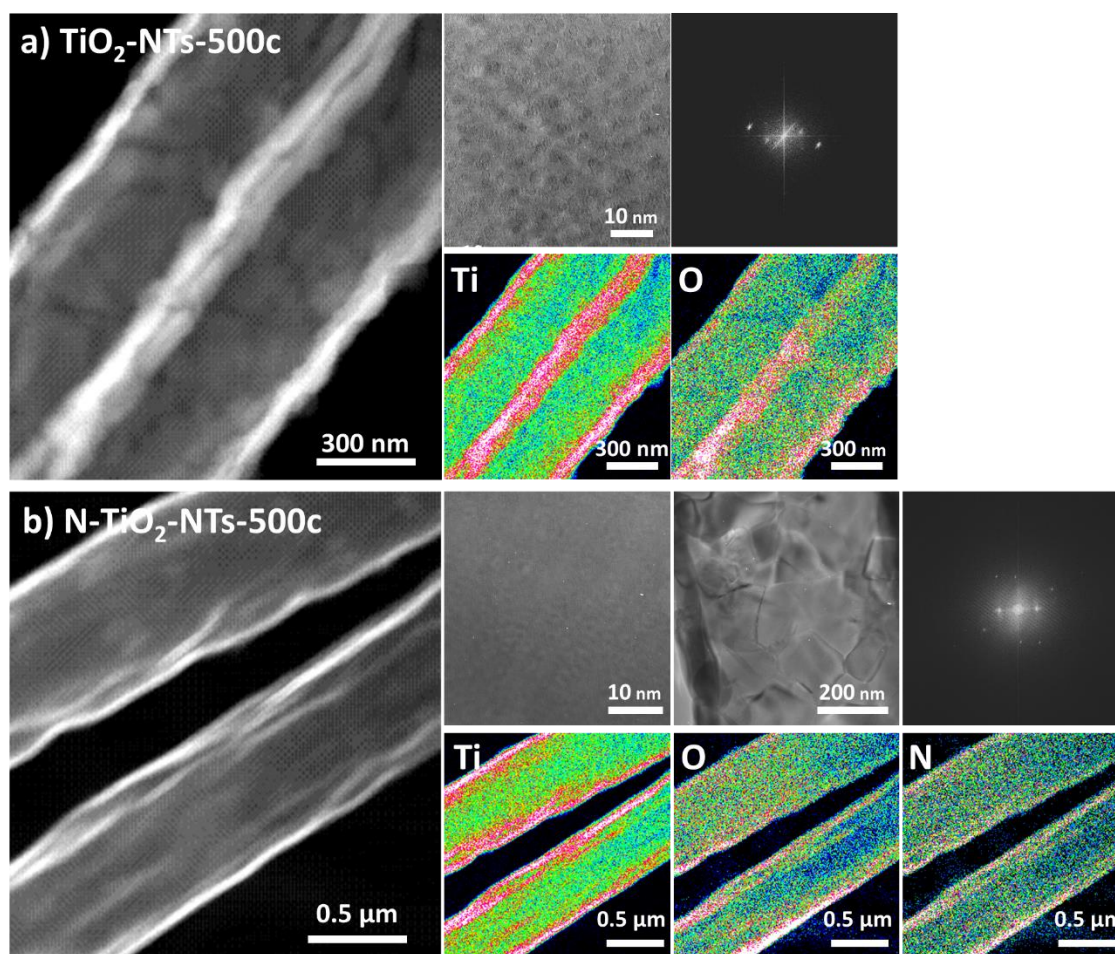
Figure 2. High resolution TEM, elemental mapping, and selected area electron diffraction images SAED of (a) TiO$_2$ NTs and (b) N-TiO$_2$ NTs (500 ALD cycles in both cases).

The crystalline structure was characterized by X-Ray Diffraction (XRD). TiO$_2$ NT samples with different thickness were composed of an anatase phase at 750 °C, as previously described[80] (**Figure 3 and S2**). TiO$_2$ NTs and N-TiO$_2$ NTs displayed the anatase crystalline structure peaks at 2θ = 25.3, 36.9, 37.7, 38.5, 48.0, 53.8, 55.0, 62.6, 68.7, 70.2, 74.9 and 75.9° [81] that corresponded to the anatase phase planes (101), (004), (200), (105), (211), (204), (116) and (107) (JCPDS-00-071-1167), respectively[82]. The anatase phase was more active than the rutile phase due to the presence of an indirect bandgap in the anatase crystal that increased the electron-hole pair separation[83]. In N-TiO$_2$ NTs, the anatase peaks were slightly shifted compared with TiO$_2$ NTs, possibly due to N incorporation in TiO$_2$ bulk or crystal lattice, as confirmed by XPS[84]. Unlike B/N co-doping, N-doping inhibits the rutile phase formation. Co-doping with B and N (B/N-TiO$_2$ NTs) led to the appearance of additional peaks [85,86]. The peak at 2θ = 28.0° was associated with the rutile phase of the (110) plane[87]. It was reported

elsewhere that the rutile phase formation is linked to the percentage of B incorporation into TiO_2[88]. Lastly, in TiO_2 NFs, both anatase and rutile phases were observed with the rutile phase diffraction peaks (1 1 0), (1 0 1), (1 1 1), (2 1 0), (2 1 1), (2 2 0), (3 1 0) and (1 1 2) (rutile TiO_2, JCPDS 21-1276)[89]. TiO_2 NFs did not show the same crystallinity as TiO_2 NTs, since the crystalline nature of TiO_2 varies with synthesizing techniques and parameters[90].
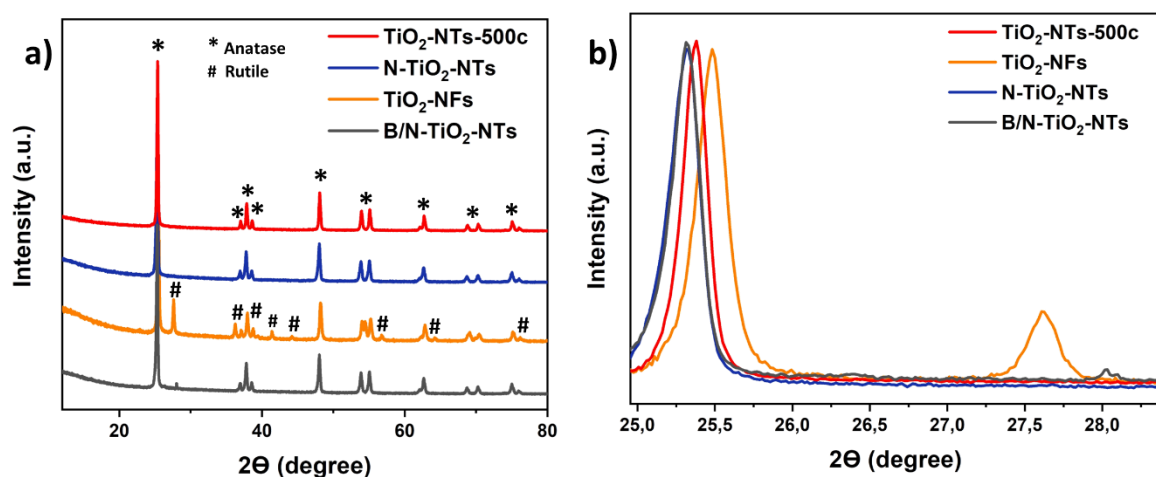

Figure 3. XRD analysis of doped and non-doped TiO_2 NTs (500 ALD cycles) and of TiO_2 NFs (a) from 15 to 80° and (b) zoom on the peaks from 24 to 29°.

To understand the effect of the different morphologies and modifications on TiO_2 structure, the percentage of anatase/rutile phase and the crystallite sizes were calculated using the Spurr (4) and Scherrer (5) equations[91,92]:

$$\%R = \frac{1}{1+0.8\left[\frac{I_A(101)}{I_R(110)}\right]} \tag{4}$$

$$D = \frac{k\lambda}{\beta cos\theta} \tag{5}$$

where I_A and I_R are the integrated intensities of the anatase (101) and rutile (110) diffraction peaks, D is the mean crystallite size, K is a shape factor = 0.89, λ is the X-ray wavelength, β is the full width at half maximum of the diffraction peak, and θ is the Bragg angle.

Comparison of the percentage of anatase/rutile phases and their particle sizes in all samples (**Table 1**) showed that in TiO_2 NT samples, doping decreased the crystallite size due to B and N inhibitory effect on the grain growth of TiO_2 particles. The anatase particle size of

non-doped TiO_2 NTs and N-TiO_2 NTs were 37.2 nm and 29.9 nm, respectively. This is probably due to the crystal lattice deformation and oxygen vacancies left by the substitution of O atoms by N atoms. The particle size decrease allows the photo-generated electrons to move faster to the TiO_2 surface and consequently it improves the catalyst degradation efficiency[67,93]. In TiO_2 NFs, the crystallite sizes of the anatase and rutile phases were 30.9 and 34.3 nm, respectively. Previous works showed that the rutile phase displays lower photocatalytic activity than the anatase phase[94].

Then, TEM and XPS were used to better describe the morphology of non-doped TiO_2 NTs and N-doped TiO_2 NTs compared with TiO_2-NFs.

Table 1: Percentage of anatase and rutile phases and crystallite sizes of the indicated samples.

Sample	Anatase (A) phase (%)	Rutile (R) phase (%)	Crystallite size (A) (nm)*	Crystallite size (R) (nm)*
TiO_2 NTs (500 AD cycles)	100.0	-	37.2	-
TiO_2 NTs (1000 ALD cycles)	100.0	-	42.1	-
TiO_2 NFs	24.5	75.5	30.9	34.3
B/N-TiO_2 NTs	91.0	9.0	32.1	46.5
N-TiO_2 NTs	100.0	-	29.9	-

*The error on the crystallite size is lower than ± 0.01%

The XPS survey of N-TiO_2 NTs confirmed the presence of Ti, O, C and N (**Figure 4a**). Carbon detection could be due to the presence of residues after calcination and PAN NF removal. The high-resolution XPS spectra of Ti 2p and of O 1s included two peaks (at 458.4 for Ti 2p3/2 and at 464.1 eV for Ti 2p1/2) and three peaks (at 529.5, 530.6 and 532.3 eV), respectively. The binding energies of Ti 2p and O 1s for TiO_2 NTs (Erreur ! Source du renvoi introuvable.) were lower than those of doped TiO_2 NTs, unlike previous literature data showing that N-doping decreases the binding energy values[95,96]. These reports demonstrated the presence of oxygen vacancies due to O substitution by N. Conversely, in our samples, the N peak (**Figure 4d**) at 399.9 eV was assigned to the presence of interstitial N atoms in the O–Ti–N environment, and not to substitutional doping of TiO_2 lattice by N. The N-O interaction in TiO_2 NT lattice increases the binding energy of the N 1s level, in agreement with our results[97]. Moreover, the existence of Ti-N bonds could be excluded because N1s would be located at lower binding energies

(<397 eV)[71,98]. This result might be interesting for photocatalytic applications because N-doping in TiO_2 NTs without Ti–N bonding causes visible-light sensitization. The total N amount in $N-TiO_2$ NTs was ~0.7%. Conversely, in $B/N-TiO_2$-NTs, B and N amounts were estimated at 6.6 and 1.3%, respectively. The higher N amount in the co-doped samples could be explained by the different doping method used. Only one peak at 192.3 eV was attributed to B 1s (**Figure 4e**), suggesting the presence of B-O-Ti groups[99]. The absence of B-N linkages indicates that $B/N-TiO_2$-NTs were not doped by BN, but co-doped by B and N. The N 1s peak at 398.2 eV (N 1s A) was explained by the substitutional N atom that replaced one O atom in the TiO_2 lattice. The peak at 401.5 (N 1s B) eV corresponded to NH_4^+ ions at the TiO_2 surface[100]. The N atom location in the TiO_2 lattice depended on the synthetic route of N-doped TiO_2.
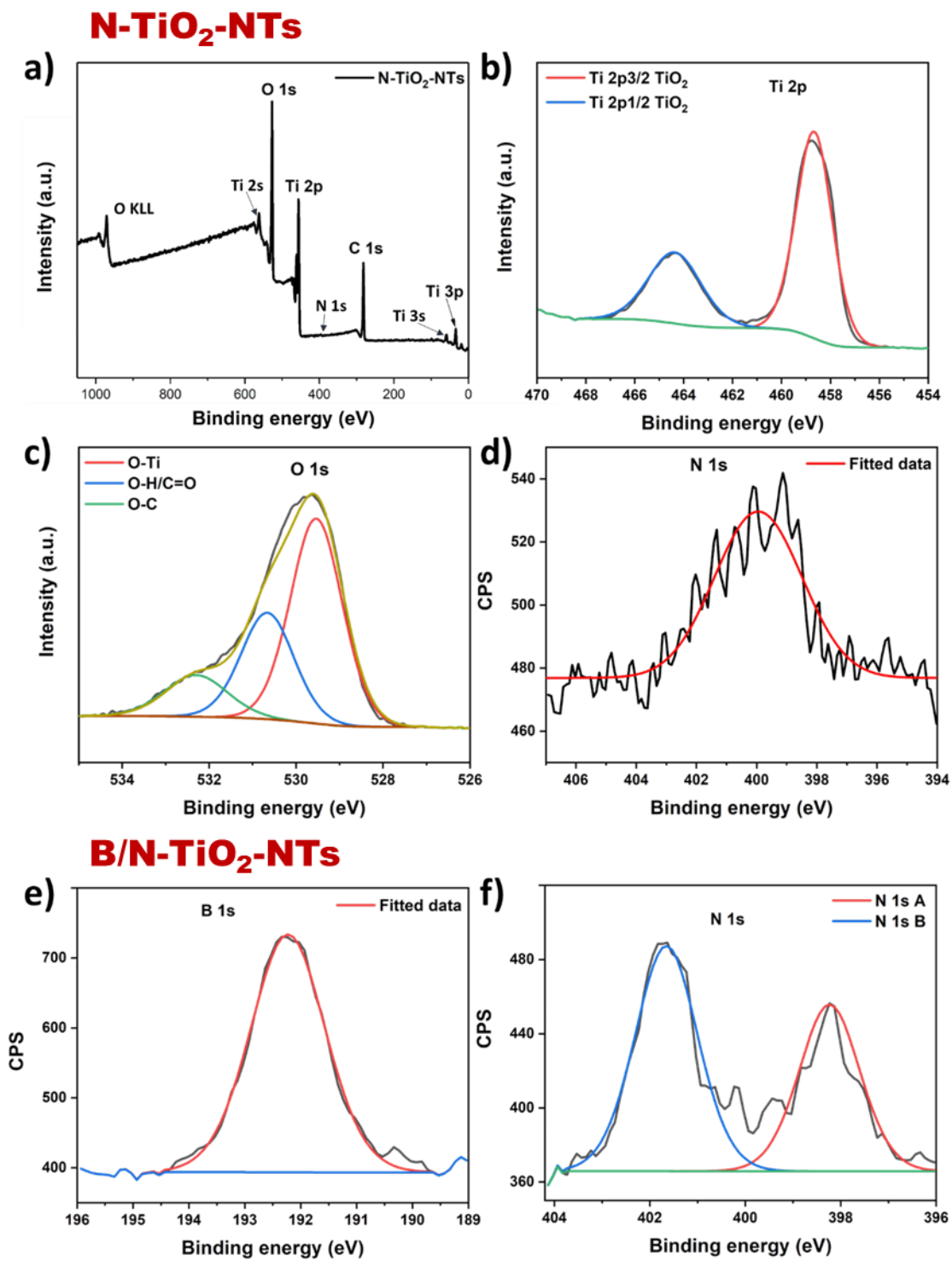
Figure 4. XPS spectra of N-TiO$_2$ NTs: (a) Survey spectra, (b) Ti 2p, (c) O 1s, (d) N 1s; and of B/N-TiO$_2$-NTs: (e) B1s and (f) N1s.

3.2. Electrochemical measurements

The fabrication of catalysts with low electron-hole pair recombination rate and high electron-charge transport is crucial for enhancing their degradation efficiency under visible light. Photoluminescence (Erreur ! Source du renvoi introuvable.), EIS and EAS measurements were carried out to investigate the interfacial charge transport process. The Nyquist plots of TiO_2 NTs, TiO_2 NFs, N-TiO_2 NTs and B/N-TiO_2 NTs are shown in **Figure 5 (a).** The Nyquist plot of TiO_2 is described by its semicircle frequency region related to the electron transfer from the TiO_2 conduction band to the electrolyte[101]. The radius arc resistance is directly correlated to the catalyst charge transportability and is determined based on the electrical model given in **Figure 5 (a)** in which R_1 is the electrolyte resistance and R_2 the charge transfer resistance. N-TiO_2 NTs displayed the lowest radius arc (i.e. R_2 value) among all samples, indicating higher charge transport and very low recombination rate. Calculation of the charge transfer resistance values (R_2) (**Table 2**) confirmed that N-TiO_2 NTs had the lowest R_2 (15.22 kΩ vs 19.11 kΩ for non-doped TiO_2 NTs and 16.52 kΩ for TiO_2 NFs). This suggests that N-doping decreases TiO_2 surface resistance and delays charge recombination at the TiO_2-electrolyte interface. Concerning TiO_2 morphology (NTs vs NFs), TiO_2 NFs showed better electron-hole pair separation resistance (*i.e.* lower R_2 than non-doped TiO_2 NTs), possibly due to their higher crystallinity that favors the charge carrier separation and transport[25]. Co-doping affected negatively the charging kinetics, indicating the occurrence of trap states and recombination centers[102]. CV with $[Fe(CN)_6]^{3-}/[Fe(CN)_6]^{4-}$ were used to investigate the effect of morphology and doping on the electrochemical response (**Figure 5b** and **Table 2**). Concerning the morphology, the current density peak was higher in TiO_2 NFs than TiO_2 NTs, possibly because of their higher EAS (Table 2)**,** despite their slightly higher ΔE_{peak}. N-doping led to the highest current density response towards $[Fe(CN)_6]^{3/4}$ and lower ΔE_{peak} , suggesting higher electrode reaction rate.

Table 2: Electrochemical results for TiO_2 NTs, TiO_2 NFs, B/N-TiO_2 NTs, and N TiO_2 NTs.

Sample	R_2 (kΩ)	Ip (A.cm^{-2})	ΔE (mV)	EAS (cm^2)

TiO$_2$ NTs	19.11	1.86±0.02	0.38	1.78±0.01
TiO$_2$ NFs	16.52	1.94±0.01	0.43	1.85±0.02
B/N-TiO$_2$ NTs	51.35	2.01±0.01	0.40	1.90±0.01
N-TiO$_2$ NTs	15.22	2.50±0.03	0.37	2.40±0.04

The $\Delta E = E_{anode} - E_{cathode}$ values showed that the mean peak-to-peak separation was shorter in N-TiO$_2$ NTs (0.3711 mV at V= 20 mV/s). When ΔE is shorter, electron transfer is faster in the redox reaction and the electrode surface is more conductive. The EAS values were 1.78 (TiO$_2$ NTs, 500 ALD cycles), 1.85 (TiO$_2$ NFs), 1.90 (B/N-TiO$_2$ NTs), and 2.40 cm^2 (N-TiO$_2$ NTs)[103]. This confirmed that doping plays a major role in enhancing TiO$_2$ photocatalytic activity by improving the electron-hole pair separation, as confirmed by the photoluminescence results. According to the literature, a smaller grain size increases the number of active surface sites and also the surface charge carrier transfer rate in 1D structured photocatalysts, leading to higher photocatalytic activity[104]. N-TiO$_2$ NTs had the smallest crystallite grain size compared with TiO$_2$ NFs, non-doped TiO$_2$ NTs and B/N co-doped TiO$_2$ NTs. It is worth noted that TiO$_2$ photocatalytic performance is influenced not only by one factor but different factors in the same time such as particle size, specific surface area, porous structure, crystalline phase, and exposed surface facets. All these parameters should be assessed to understand the catalytic performance of the material.
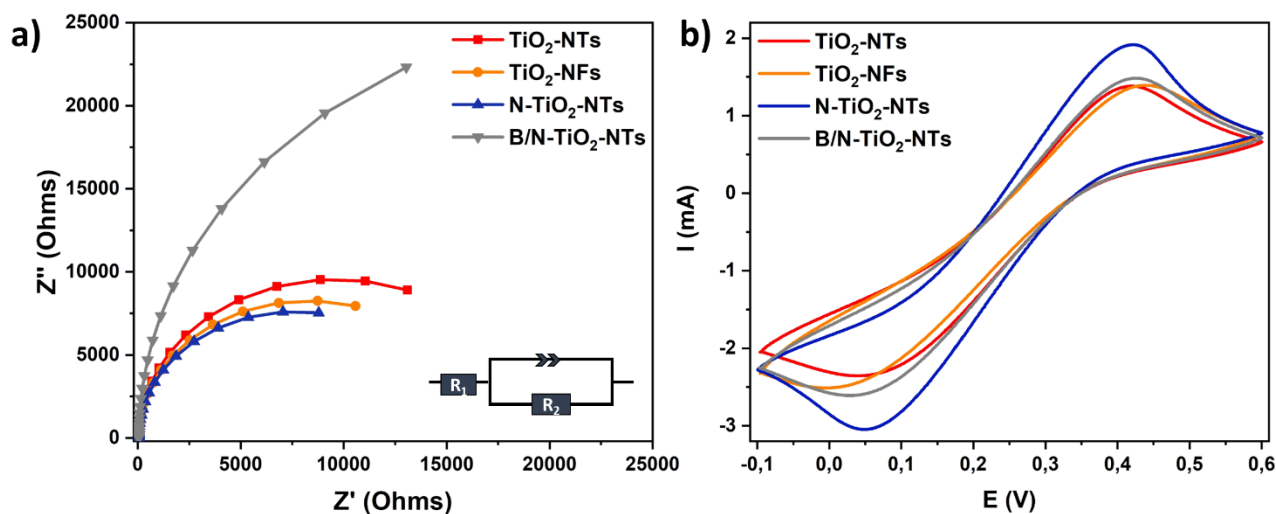
Figure 5. a) Nyquist plots and b) Cyclic voltammograms, obtained in potassium hexacyanoferrate solution with a scan rate of 20 mV/s, for TiO$_2$ NTs, TiO$_2$ NFs, N-TiO$_2$ NTs, and B/N-TiO$_2$ NTs (surface= 1 cm^2).

3.3.   Photocatalytic experiments

3.3.1. Photocatalytic degradation

Visible light photodegradation of acetaminophen (**Figure 6**) was compared using different TiO$_2$-based catalysts. This showed that higher number of ALD cycles increased the wall thickness (not presented in this paper) that strongly affected acetaminophen degradation efficiency (**Figure 6a**), in agreement with the litterature[80]. The highest degradation efficiency was obtained with TiO$_2$ NTs prepared using 500 ALD cycles compared with 800 and 1000 ALD cycles: 95.7% after 90 minutes of visible light irradiation versus 76.6% and 56.0%, respectively. On the basis of these results, TiO$_2$ NTs fabricated using 500 ALD cycles were used for all the other experiments. As the catalyst morphology plays a major role in the degradation of pharmaceutical pollutants, it was important to understand the effects of the surface area, crystallinity, electron-hole pair recombination, and bandgap on the photocatalytic properties[95]. The visible light catalytic properties of TiO$_2$ NFs (fabricated by electrospinning followed by calcination at 750°C for 4h) were compared with those of TiO$_2$ NTs (**Figure 6**). As

N-TiO$_2$ NTs have lower recombination rate and higher surface area than TiO$_2$ NFs (see EIS and EAS data), their photocatalytic activity was higher. It was previously reported that anatase TiO$_2$ displays higher degradation efficiency than a catalyst with both crystalline phases[80,93]. Wang *et al.* observed better photocatalytic degradation of methylene blue by TiO$_2$ nanosheets than TiO$_2$ nanoparticles, highlighting the importance of the catalyst structure. Moreover, they reported that higher surface area further improves degradation under visible light[105].

Then, different TiO$_2$ NT samples were prepared by varying the dopant nature to explore how to limit the recombination of photogenerated electron-hole pairs for feasible charge separation and transfer, and how to expand the absorption edge to the visible light range. After 90 minutes of visible light exposure, 98.3%, 95.7% and 31.9% of acetaminophen were degraded in the presence of N-TiO$_2$ NTs, TiO$_2$ NTs, and B/N-TiO$_2$ NTs, respectively (Erreur ! Source du renvoi introuvable.). This indicates the N-doping better increase the degradation efficiency compared with B and D co-doping. This modification step might be affected by many factors, including the type and level of N-doping and the concentration of O$_2$ vacancies, and this will greatly influence the photocatalytic activity[106,107].

The positive effect of N-doping on TiO$_2$ catalyst properties has been widely reported. Indeed, N-doping creates O$_2$ vacancies that participate in trapping the photoinduced electrons and act as a reactive center for the photocatalytic process. As the number of articles on TiO$_2$ modification by N-doping is too high, comparing their results is complicated due to the many different experimental conditions (e.g. catalyst structure, concentrations, matrix, lamp source)[69,93,108–110].
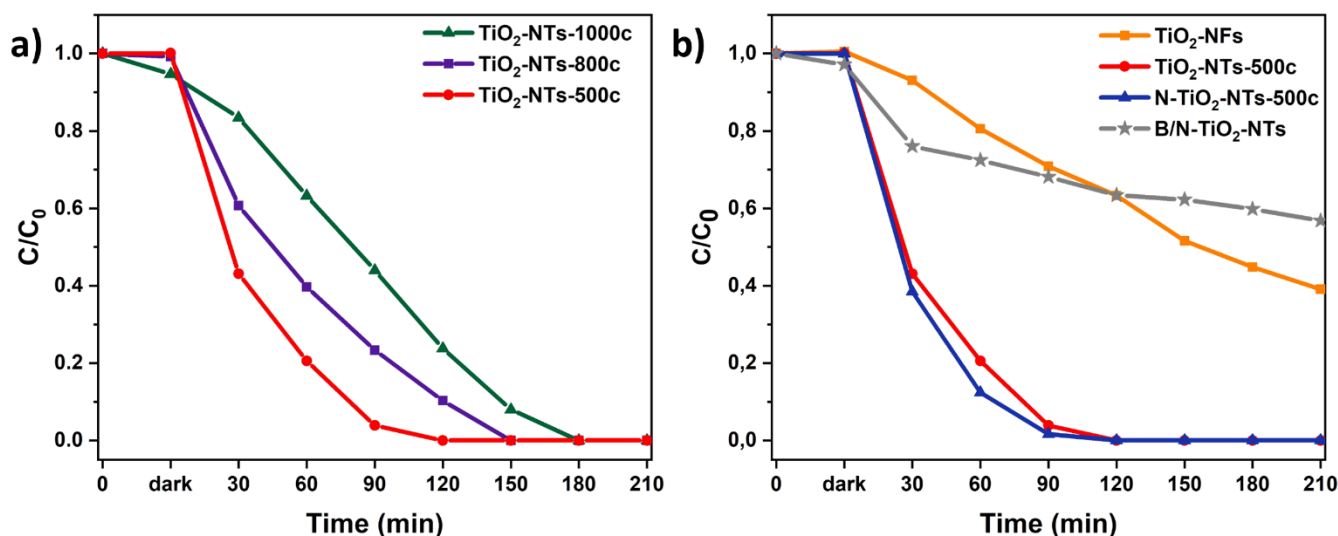
Figure 6. Acetaminophen degradation under visible light in function of a) TiO_2 wall thickness (number of ALD cycles), b) TiO_2 structure, morphology, and doping.

3.3.2. Photocatalytic kinetic model

The photocatalytic degradation of acetaminophen under visible light followed a pseudo-first-order kinetics. Indeed, the closely linear relationship between $\ln(C_0/C)$ and irradiation time (t) fits well with the first-order reaction rate of acetaminophen degradation (**Figure 7a**). The degradation rate in the presence of N-TiO_2 NTs was 0.045 min^{-1}, which is 4 times higher than with TiO_2 NFs. This result was in agreement with the lower electron-hole pair recombination rate (photoluminescence and EIS measurements). Moreover, the high percentage of rutile phase in TiO_2 NFs decreased their degradation efficiency. In conclusion, ALD is a promising technique for fabricating catalysts with well-organized structure and good degradation performance under visible light.
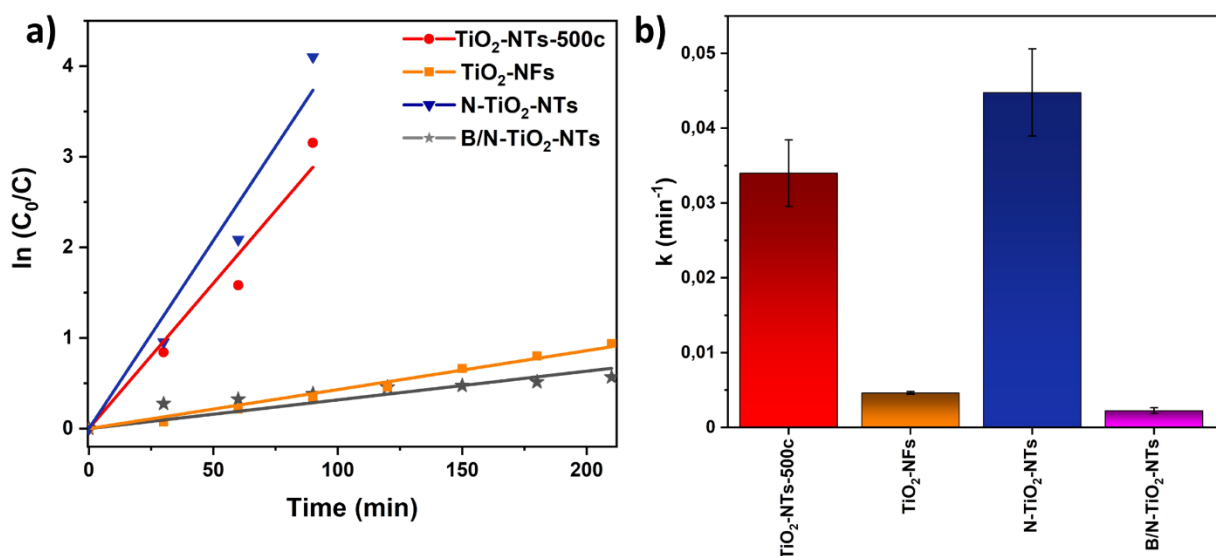
Figure 7. Photocatalytic degradation of acetaminophen by the indicated TiO_2 catalysts. a) Plot of $\ln(C_0/C)$ in function of time (fitted to first order rate law), and b) Values the first order rate constant.

3.3.3. Stability, quenching, and toxicity tests

N-TiO_2 NTs (500 ALD cycles) recyclability and stability were tested for five consecutive cycles (**Figure 8a**). After each cycle, the catalyst was rinsed several times with distilled water and dried at 70 °C before the next cycle. Acetaminophen degradation rates, after 90 min of visible light irradiation, were 98.3% (first cycle), 97.5% (second cycle), 96.0% (third cycle), 93.9% (fourth cycle), and 82.6% (fifth cycle). This indicates a slight loss of degradation efficiency over time, although acetaminophen removal was still >82% after five runs. This activity decrease might be related to N loss in the catalyst after consecutive cycles, or to the accumulation of by-products that are formed during the catalyst surface degradation, thus decreasing the available active sites[111]. Despite this loss of activity (<20%) after five cycles, N-TiO_2 NTs can be considered a promising stable catalyst material for water treatment.

Organic pollutant degradation by advanced oxidation processes can lead to the production of by-products[112,113] with cyclic and aromatic structure that are highly toxic, sometimes more than the initial pollutant. To evaluate the acute toxicity of intermediates generated during acetaminophen photodegradation, *V. fischeri* luminescence intensity variations were quantified after 15-min incubation with aqueous solution aliquots collected during acetaminophen degradation (**Figure 8b**). Acetaminophen toxicity was very low at the used

concentration, as we previously reported[114]. Toxicity strongly increased and luminescence was inhibited by ~90% after 1h of visible light irradiation. This result is consistent with previous studies showing the formation of toxic aromatic by-products (e.g. 1,4-benzoquinone, hydroquinone, benzoic acid, and benzaldehyde) during acetaminophen degradation[115–117]. Then, toxicity progressively decreased and luminescence intensity inhibition was <20% after 3h of irradiation. During this period, further oxidation of the formed molecules would result in the breakdown of their aromatic structures. After 6h of irradiation, when short-chain carboxylic acids are converted into CO_2 and H_2O, the luminescence inhibition rate was <5%.
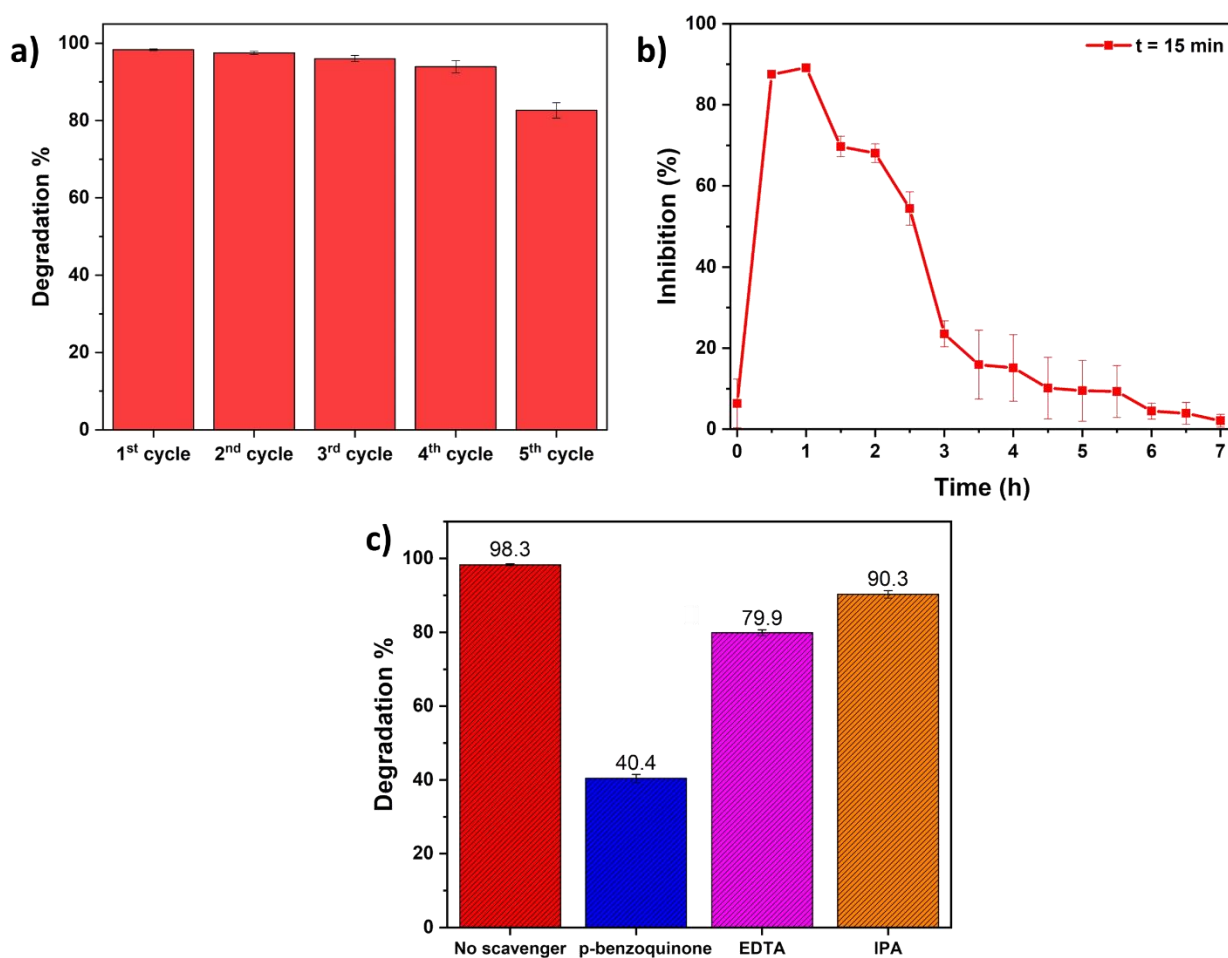

Figure 8. a) Reusability of N–TiO$_2$-NTs for photocatalytic activity. b) Inhibition of of *V. fischeri* luminescence emission during acetaminophen photodegradation. c) Effect of radical scavengers on acetaminophen degradation.

During photodegradation, OH° radicals, h^+ and O_2^- radicals are generally considered as active species. To determine their contribution to acetaminophen degradation, scavenger tests were performed using EDTA (h^+ scavenger), isopropanol (OH radicals). and p-benzoquinone (O_2^- radicals) and N-TiO$_2$ NTs as catalyst. The results (**Figure 8c**) suggested that all three active radical species are implicated in acetaminophen degradation because all scavengers decreased its photodegradation, particularly p-benzoquinone (O_2^- radical scavenger) that reduced acetaminophen degradation rate from 98.3% to 40.4%.

4.   Conclusion

In this work, we first compared the photocatalytic properties of two different 1D TiO$_2$ structures fabricated using two different approaches. TiO$_2$ NTs, synthesized by ALD, displayed 3 times higher acetaminophen degradation rates (after 90 min of visible light irradiation) than TiO$_2$ NFs, produced by electrospinning. Then, we investigated whether non-metal doping increased TiO$_2$ NT degradation efficiency. N-doping enhanced the catalytic properties, as indicated by the degradation rate of 0.045 min^{-1} of N-TiO$_2$ NTs. This result could be explained by the lower recombination rate of the photogenerated charges and higher electroactive surface area (2.40 cm^2 in N-TiO$_2$ NTs versus 1.78 cm^2 in TiO$_2$ NTs). The recyclability results suggest that ALD is an interesting technique for preparing photocatalysts on immobilized supports with good degradation efficiency and high stability. Quenching tests indicated that superoxide radicals played a major role in acetaminophen degradation. In this work, we confirmed the higher degradation activity of highly structured 1D materials under visible light. Now, these catalysts should be tested using a real wastewater matrix with different organic pollutant to test the selectivity of the photocatalyst and the ability to degrade different types of pollutants.

References

1. Takeuchi N, Yasuoka K. Review of plasma-based water treatment technologies for the decomposition of persistent organic compounds. *Jpn J Appl Phys*. 2020;60(SA):SA0801. doi:10.35848/1347-4065/abb75d

2. Gehrke I, Geiser A, Somborn-Schulz A. Innovations in nanotechnology for water treatment. *Nanotechnol Sci Appl*. 2015;8:1-17. doi:10.2147/NSA.S43773

3. World Health Organization. Pharmaceuticals in drinking-water. Published online 2012.

4. Houtman CJ. Emerging contaminants in surface waters and their relevance for the production of drinking water in Europe. *J Integr Environ Sci*. 2010;7(4):271-295.

5. Tran NH, Reinhard M, Gin KYH. Occurrence and fate of emerging contaminants in municipal wastewater treatment plants from different geographical regions-a review. *Water Res*. 2018;133:182-207.

6. Nam SW, Jo BI, Yoon Y, Zoh KD. Occurrence and removal of selected micropollutants in a water treatment plant. *Chemosphere*. 2014;95:156-165. doi:10.1016/j.chemosphere.2013.08.055

7. Phong Vo HN, Le GK, Hong Nguyen TM, et al. Acetaminophen micropollutant: Historical and current occurrences, toxicity, removal strategies and transformation pathways in different environments. *Chemosphere*. 2019;236:124391. doi:10.1016/j.chemosphere.2019.124391

8. Stasinakis A. Use of selected advanced oxidation processes (AOPs) for wastewater treatment–a mini review. *Glob NEST J*. 2008;10(3):376-385.

9. Rodriguez-Narvaez OM, Peralta-Hernandez JM, Goonetilleke A, Bandala ER. Treatment technologies for emerging contaminants in water: A review. *Chem Eng J*. 2017;323:361-380.

10. Teodosiu C, Gilca AF, Barjoveanu G, Fiore S. Emerging pollutants removal through advanced drinking water treatment: A review on processes and environmental performances assessment. *J Clean Prod*. 2018;197:1210-1221. doi:10.1016/j.jclepro.2018.06.247

11. Friedmann D, Mendive C, Bahnemann D. TiO2 for water treatment: parameters affecting the kinetics and mechanisms of photocatalysis. *Appl Catal B Environ*. 2010;99(3-4):398-406.

12. Chong MN, Jin B, Chow CWK, Saint C. Recent developments in photocatalytic water treatment technology: A review. *Water Res*. 2010;44(10):2997-3027. doi:10.1016/j.watres.2010.02.039

13. Ameta R, Solanki MS, Benjamin S, Ameta SC. Chapter 6 - Photocatalysis. In: Ameta SC, Ameta R, eds. *Advanced Oxidation Processes for Waste Water Treatment*. Academic Press; 2018:135-175. doi:10.1016/B978-0-12-810499-6.00006-1

14. Serpone N. Photocatalysis. In: *Kirk-Othmer Encyclopedia of Chemical Technology*. American Cancer Society; 2000. doi:https://doi.org/10.1002/0471238961.1608152019051816.a01

15. Gaya UI, Abdullah AH. Heterogeneous photocatalytic degradation of organic contaminants over titanium dioxide: a review of fundamentals, progress and problems. *J Photochem Photobiol C Photochem Rev*. 2008;9(1):1-12.

16. Hong SP, Park J, SM Bhat S, et al. Comprehensive study on the morphology control of TiO2 nanorods on foreign substrates by the hydrothermal method. *Cryst Growth Des*. 2018;18(11):6504-6512.

17. Ramanavicius S, Ramanavicius A. Insights in the application of stoichiometric and non-stoichiometric titanium oxides for the design of sensors for the determination of gases and VOCs (TiO2− x and TinO2n− 1 vs. TiO2). *Sensors*. 2020;20(23):6833.

18. Ramanavicius S, Tereshchenko A, Karpicz R, et al. TiO2-x/TiO2-structure based 'self-heated' sensor for the determination of some reducing gases. *Sensors*. 2020;20(1):74.

19. Nakata K, Fujishima A. TiO2 photocatalysis: Design and applications. *J Photochem Photobiol C Photochem Rev*. 2012;13(3):169-189. doi:10.1016/j.jphotochemrev.2012.06.001

20. Nasr M, Eid C, Habchi R, Miele P, Bechelany M. Recent Progress on Titanium Dioxide Nanomaterials for Photocatalytic Applications. *ChemSusChem*. 2018;11(18):3023-3047. doi:10.1002/cssc.201800874

21. Nasr O, Mohamed O, Al-Shirbini AS, Abdel-Wahab AM. Photocatalytic degradation of acetaminophen over Ag, Au and Pt loaded TiO2 using solar light. *J Photochem Photobiol Chem*. 2019;374:185-193. doi:10.1016/j.jphotochem.2019.01.032

22. Bui XT, Chiemchaisri C, Fujioka T, Varjani S. Introduction to Recent Advances in Water and Wastewater Treatment Technologies. In: Bui XT, Chiemchaisri C, Fujioka T, Varjani S, eds. *Water and Wastewater Treatment Technologies*. Springer Singapore; 2019:3-12. doi:10.1007/978-981-13-3259-3_1

23. Xiang Q, Ma X, Zhang D, et al. Interfacial modification of titanium dioxide to enhance photocatalytic efficiency towards H2 production. *J Colloid Interface Sci*. 2019;556:376-385. doi:10.1016/j.jcis.2019.08.033

24. Bethi B, Sonawane SH, Bhanvase BA, Gumfekar SP. Nanomaterials-based advanced oxidation processes for wastewater treatment: A review. *Chem Eng Process - Process Intensif*. 2016;109:178-189. doi:10.1016/j.cep.2016.08.016

25. Akple M, Low J, Qin Z, et al. Nitrogen-doped TiO2 microsheets with enhanced visible light photocatalytic activity for CO2 reduction. *Chin J Catal*. 2015;36:2127-2134.

26. Klavarioti M, Mantzavinos D, Kassinos D. Removal of residual pharmaceuticals from aqueous systems by advanced oxidation processes. *Environ Int*. 2009;35(2):402-417.

27. Katal R, Masudy-Panah S, Tanhaei M, Farahani MHDA, Jiangyong H. A review on the synthesis of the various types of anatase TiO2 facets and their applications for photocatalysis. *Chem Eng J*. 2020;384:123384. doi:10.1016/j.cej.2019.123384

28. Ghori MZ, Veziroglu S, Henkel B, et al. A comparative study of photocatalysis on highly active columnar TiO2 nanostructures in-air and in-solution. *Sol Energy Mater Sol Cells*. 2018;178:170-178. doi:10.1016/j.solmat.2018.01.019

29. Yang HG, Liu G, Qiao SZ, et al. Solvothermal Synthesis and Photoreactivity of Anatase TiO2 Nanosheets with Dominant {001} Facets. *J Am Chem Soc*. 2009;131(11):4078-4083. doi:10.1021/ja808790p

30. Ramakrishnan VM, Natarajan M, Santhanam A, Asokan V, Velauthapillai D. Size controlled synthesis of TiO2 nanoparticles by modified solvothermal method towards effective photo catalytic and photovoltaic applications. *Mater Res Bull*. 2018;97:351-360. doi:10.1016/j.materresbull.2017.09.017

31. Mamaghani AH, Haghighat F, Lee CS. Role of titanium dioxide (TiO2) structural design/morphology in photocatalytic air purification. *Appl Catal B Environ*. 2020;269:118735. doi:10.1016/j.apcatb.2020.118735

32. El-Maghrabi HH, Barhoum A, Nada AA, et al. Synthesis of mesoporous core-shell CdS@TiO2 (0D and 1D) photocatalysts for solar-driven hydrogen fuel production. *J Photochem Photobiol Chem*. 2018;351:261-270. doi:10.1016/j.jphotochem.2017.10.048

33. Ramanavicius S, Ramanavicius A. Progress and Insights in the Application of MXenes as New 2D Nano-Materials Suitable for Biosensors and Biofuel Cell Design. *Int J Mol Sci*. 2020;21(23). doi:10.3390/ijms21239224

34. Rosales M, Zoltan T, Yadarola C, Mosquera E, Gracia F, García A. The influence of the morphology of 1D TiO2 nanostructures on photogeneration of reactive oxygen species and enhanced photocatalytic activity. *J Mol Liq*. 2019;281:59-69. doi:10.1016/j.molliq.2019.02.070

35. Guo MY, Fung MK, Fang F, et al. ZnO and TiO2 1D nanostructures for photocatalytic applications. *J Alloys Compd*. 2011;509(4):1328-1332. doi:10.1016/j.jallcom.2010.10.028

36. Erdogan N, Park J, Choi W, Kim SY, Ozturk A. Alkaline hydrothermal synthesis, characterization, and photocatalytic activity of TiO2 nanostructures: the effect of initial TiO2 phase. *J Nanosci Nanotechnol*. 2019;19(3):1511-1519.

37. Ge M, Li Q, Cao C, et al. One-dimensional TiO2 Nanotube Photocatalysts for Solar Water Splitting. *Adv Sci*. 2017;4(1):1600152. doi:10.1002/advs.201600152

38. Feng T, Feng GS, Yan L, Pan JH. One-dimensional nanostructured TiO2 for photocatalytic degradation of organic pollutants in wastewater. *Int J Photoenergy*. 2014;2014.

39. Shahrezaei M, Babaluo AA, Habibzadeh S, Haghighi M. Photocatalytic properties of 1D TiO2 nanostructures prepared from polyacrylamide gel–TiO2 nanopowders by hydrothermal synthesis. *Eur J Inorg Chem*. 2017;2017(3):694-703.

40. Chatzitakis A, Grandcolas M, Xu K, et al. Assessing the photoelectrochemical properties of C, N, F codoped TiO2 nanotubes of different lengths. *Sel Contrib 9th Eur Meet Sol Chem Photocatal Environ Appl SPEA-9*. 2017;287:161-168. doi:10.1016/j.cattod.2016.11.040

41. Roy P, Berger S, Schmuki P. TiO2 nanotubes: synthesis and applications. *Angew Chem Int Ed*. 2011;50(13):2904-2939.

42. Paramasivam I, Jha H, Liu N, Schmuki P. A review of photocatalysis using self-organized TiO2 nanotubes and other ordered oxide nanostructures. *small*. 2012;8(20):3073-3103.

43. Zhu S, Nie L. Progress in fabrication of one-dimensional catalytic materials by electrospinning technology. *J Ind Eng Chem*. 2021;93:28-56. doi:10.1016/j.jiec.2020.09.016

44. Kowalski D, Kim D, Schmuki P. TiO2 nanotubes, nanochannels and mesosponge: Self-organized formation and applications. *Nano Today*. 2013;8(3):235-264. doi:10.1016/j.nantod.2013.04.010

45. Meng X, Banis MN, Geng D, et al. Controllable atomic layer deposition of one-dimensional nanotubular TiO2. *Appl Surf Sci*. 2013;266:132-140. doi:10.1016/j.apsusc.2012.11.116

46. Liang HC, Li XZ, Nowotny J. Photocatalytical properties of TiO2 nanotubes. In: Vol 162. Trans Tech Publ; 2010:295-328.

47. Weber M, Julbe A, Kim SS, Bechelany M. Atomic layer deposition (ALD) on inorganic or polymeric membranes. *J Appl Phys*. 2019;126(4):041101. doi:10.1063/1.5103212

48. George SM. Atomic Layer Deposition: An Overview. *Chem Rev*. 2010;110(1):111-131. doi:10.1021/cr900056b

49. Elias J, Utke I, Yoon S, et al. Electrochemical growth of ZnO nanowires on atomic layer deposition coated polystyrene sphere templates. *Electrochem Adv Mater Technol Instrum*. 2013;110:387-392. doi:10.1016/j.electacta.2013.04.168

50. Abi Younes P, Sayegh S, Nada AA, et al. Elaboration of porous alumina nanofibers by electrospinning and molecular layer deposition for organic pollutant removal. *Colloids Surf Physicochem Eng Asp*. 2021;628:127274. doi:10.1016/j.colsurfa.2021.127274

51. Najem M, Nada AA, Weber M, et al. Palladium/Carbon Nanofibers by Combining Atomic Layer Deposition and Electrospinning for Organic Pollutant Degradation. *Materials*. 2020;13(8). doi:10.3390/ma13081947

52. Kim WS, Lee BS, Kim DH, Kim HC, Yu WR, Hong SH. SnO2 nanotubes fabricated using electrospinning and atomic layer deposition and their gas sensing performance. *Nanotechnology*. 2010;21(24):245605.

53. Kim GM, Lee SM, Michler G, Roggendorf H, Gosele U, Knez M. Nanostructured pure anatase titania tubes replicated from electrospun polymer fiber templates by atomic layer deposition. *Chem Mater*. 2008;20(9):3085-3091.

54. Szilágyi IM, Nagy D. Review on one-dimensional nanostructures prepared by electrospinning and atomic layer deposition. *J Phys Conf Ser*. 2014;559:012010. doi:10.1088/1742-6596/559/1/012010

55. McClure CD, Oldham CJ, Walls HJ, Parsons GN. Large effect of titanium precursor on surface reactivity and mechanical strength of electrospun nanofibers coated with TiO2 by atomic layer deposition. *J Vac Sci Technol Vac Surf Films*. 2013;31(6):061506.

56. Su CY, Wang LC, Liu WS, Wang CC, Perng TP. Photocatalysis and Hydrogen Evolution of Al- and Zn-Doped TiO2 Nanotubes Fabricated by Atomic Layer Deposition. *ACS Appl Mater Interfaces*. 2018;10(39):33287-33295. doi:10.1021/acsami.8b12299

57. Lee SY, Park SJ. TiO2 photocatalyst for water treatment applications. *J Ind Eng Chem*. 2013;19(6):1761-1769.

58. Fang W, Xing M, Zhang J. Modifications on reduced titanium dioxide photocatalysts: A review. *J Photochem Photobiol C Photochem Rev*. 2017;32:21-39.

59. Fujishima A, Zhang X, Tryk DA. TiO2 photocatalysis and related surface phenomena. *Surf Sci Rep*. 2008;63(12):515-582. doi:10.1016/j.surfrep.2008.10.001

60. Khaki MRD, Shafeeyan MS, Raman AAA, Daud WMAW. Application of doped photocatalysts for organic pollutant degradation - A review. *J Environ Manage*. 2017;198:78-94. doi:10.1016/j.jenvman.2017.04.099

61. Mrowetz M, Balcerski W, Colussi A, Hoffmann MR. Oxidative power of nitrogen-doped TiO2 photocatalysts under visible illumination. *J Phys Chem B*. 2004;108(45):17269-17273.

62. Park JH, Kim S, Bard AJ. Novel carbon-doped TiO2 nanotube arrays with high aspect ratios for efficient solar water splitting. *Nano Lett*. 2006;6(1):24-28.

63. Tachikawa T, Tojo S, Kawai K, et al. Photocatalytic Oxidation Reactivity of Holes in the Sulfur- and Carbon-Doped TiO2 Powders Studied by Time-Resolved Diffuse Reflectance Spectroscopy. *J Phys Chem B*. 2004;108(50):19299-19306. doi:10.1021/jp0470593

64. Takeshita K, Yamakata A, Ishibashi T aki, Onishi H, Nishijima K, Ohno T. Transient IR absorption study of charge carriers photogenerated in sulfur-doped TiO2. *J Photochem Photobiol Chem*. 2006;177(2-3):269-275.

65. Ohno T, Akiyoshi M, Umebayashi T, Asai K, Mitsui T, Matsumura M. Preparation of S-doped TiO2 photocatalysts and their photocatalytic activities under visible light. *Appl Catal Gen*. 2004;265(1):115-121.

66. Liu R, Yang F, Xie Y, Yu Y. Visible-light responsive boron and nitrogen codoped anatase TiO2 with exposed {0 0 1} facet: Calculation and experiment. *Appl Surf Sci*. 2019;466:568-577.

67. Wang SQ, Liu WB, Fu P, Cheng WL. Enhanced photoactivity of N-doped TiO2 for Cr(VI) removal: Influencing factors and mechanism. *Korean J Chem Eng*. 2017;34(5):1584-1590. doi:10.1007/s11814-017-0003-7

68. Dong F, Wang H, Wu Z, Qiu J. Marked enhancement of photocatalytic activity and photochemical stability of N–doped TiO2 nanocrystals by Fe3+/Fe2+ surface modification. *J Colloid Interface Sci*. 2010;343(1):200-208. doi:10.1016/j.jcis.2009.11.012

69. Zhang Z, Wang X, Long J, Gu Q, Ding Z, Fu X. Nitrogen-doped titanium dioxide visible light photocatalyst: Spectroscopic identification of photoactive centers. *J Catal*. 2010;276(2):201-214. doi:10.1016/j.jcat.2010.07.033

70. Huang J, Dou L, Li J, Zhong J, Li M, Wang T. Excellent visible light responsive photocatalytic behavior of N-doped TiO2 toward decontamination of organic pollutants. *J Hazard Mater*. 2021;403:123857. doi:10.1016/j.jhazmat.2020.123857

71. Kertmen A, Barbé E, Szkoda M, et al. Photoelectrochemically Active N-Adsorbing Ultrathin TiO2 Layers for Water-Splitting Applications Prepared by Pyrolysis of Oleic Acid

on Iron Oxide Nanoparticle Surfaces under Nitrogen Environment. *Adv Mater Interfaces*. 2019;6(3):1801286. doi:10.1002/admi.201801286

72. Chen C, Ma W, Zhao J. Photocatalytic degradation of organic pollutants by co-doped TiO2 under visible light irradiation. *Curr Org Chem*. 2010;14(7):630-644.

73. Sayegh S, Tanos F, Nada A, et al. Tunable TiO 2–BN–Pd nanofibers by combining electrospinning and atomic layer deposition to enhance photodegradation of acetaminophen. *Dalton Trans*. 2022;51(7):2674-2695.

74. Lin L, Lin L, Jiang W, Bechelany M, Nasr M, Jarvis J. Adsorption and photocatalytic oxidation of ibuprofen using nanocomposites of TiO2 nanofibers combined with BN nanosheets : Degradation products and mechanisms Chemosphere Adsorption and photocatalytic oxidation of ibuprofen using nanocomposites of TiO 2 n. *Chemosphere*. 2019;220(December 2018):921-929. doi:10.1016/j.chemosphere.2018.12.184

75. Konstantinou IK, Albanis TA. TiO2-assisted photocatalytic degradation of azo dyes in aqueous solution: kinetic and mechanistic investigations: A review. *Appl Catal B Environ*. 2004;49(1):1-14. doi:10.1016/j.apcatb.2003.11.010

76. Konstantinou IK, Albanis TA. Photocatalytic transformation of pesticides in aqueous titanium dioxide suspensions using artificial and solar light: intermediates and degradation pathways. *Appl Catal B Environ*. 2003;42(4):319-335. doi:10.1016/S0926-3373(02)00266-7

77. Xuan T, Le H, Nguyen T Van, et al. Chemosphere Correlation between degradation pathway and toxicity of acetaminophen and its by-products by using the electro-Fenton process in aqueous media. 2017;172:1-9. doi:10.1016/j.chemosphere.2016.12.060

78. Borbón-Nuñez HA, Dominguez D, Muñoz-Muñoz F, et al. Fabrication of hollow TiO2 nanotubes through atomic layer deposition and MWCNT templates. *Powder Technol*. 2017;308:249-257. doi:10.1016/j.powtec.2016.12.001

79. Lazar MA, Varghese S, Nair SS. Photocatalytic Water Treatment by Titanium Dioxide: Recent Updates. *Catalysts*. 2012;2(4). doi:10.3390/catal2040572

80. Wang CC, Kei CC, Perng TP. Fabrication of TiO2 nanotubes by atomic layer deposition and their photocatalytic and photoelectrochemical applications. *Nanotechnology*. 2011;22(36):365702.

81. López de Dicastillo C, Patiño C, Galotto MJ, Palma JL, Alburquenque D, Escrig J. Novel Antimicrobial Titanium Dioxide Nanotubes Obtained through a Combination of Atomic Layer Deposition and Electrospinning Technologies. *Nanomaterials*. 2018;8(2). doi:10.3390/nano8020128

82. Thamaphat K, Limsuwan P, Ngotaworntchai B. Phase characterization of TiO2 powder by XRD and TEM. *Agric Nat Resour*. 2008;42(5):357-361.

83. Soo JZ, Lee KM, Ang BC, Ong BH. Optimal electrospun TiO2 nanofiber photocatalytic performance via synergistic morphology and particle crystallinity with anatase/rutile phase tuning. *Phys Status Solidi A*. 2019;216(16):1900066.

84. Sinha I, De AK. Chapter 1 - An overview of synthesis techniques for preparing doped photocatalysts. In: Singh P, Borthakur A, Mishra PK, Tiwary D, eds. *Nano-Materials as Photocatalysts for Degradation of Environmental Pollutants*. Elsevier; 2020:1-13. doi:10.1016/B978-0-12-818598-8.00001-8

85. Lu N, Quan X, Li J, Chen S, Yu H, Chen G. Fabrication of Boron-Doped TiO2 Nanotube Array Electrode and Investigation of Its Photoelectrochemical Capability. *J Phys Chem C*. 2007;111(32):11836-11842. doi:10.1021/jp071359d

86. Szkoda M, Lisowska-Oleksiak A, Siuzdak K. Optimization of boron-doping process of titania nanotubes via electrochemical method toward enhanced photoactivity. *J Solid State Electrochem*. 2016;20(6):1765-1774. doi:10.1007/s10008-016-3185-8

87. Natarajan TS, Natarajan K, Bajaj HC, Tayade RJ. Enhanced photocatalytic activity of bismuth-doped TiO 2 nanotubes under direct sunlight irradiation for degradation of Rhodamine B dye. *J Nanoparticle Res*. 2013;15(5):1-18.

88. Gombac V, De Rogatis L, Gasparotto A, et al. TiO2 nanopowders doped with boron and nitrogen for photocatalytic applications. *Doping Funct Photoactive Semicond Met Oxides*. 2007;339(1):111-123. doi:10.1016/j.chemphys.2007.05.024

89. Doh SJ, Kim C, Lee SG, Lee SJ, Kim H. Development of photocatalytic TiO2 nanofibers by electrospinning and its application to degradation of dye pollutants. *J Hazard Mater*. 2008;154(1):118-127. doi:10.1016/j.jhazmat.2007.09.118

90. Yu J, Yu H, Cheng B, Trapalis C. Effects of calcination temperature on the microstructures and photocatalytic activity of titanate nanotubes. *J Mol Catal Chem*. 2006;249(1):135-142. doi:10.1016/j.molcata.2006.01.003

91. Yang Z, Shi Y, Wang B. Photocatalytic activity of magnetically anatase TiO2 with high crystallinity and stability for dyes degradation: Insights into the dual roles of SiO2 interlayer between TiO2 and CoFe2O4. *Appl Surf Sci*. 2017;399:192-199. doi:10.1016/j.apsusc.2016.12.078

92. Jin X, Yuan K, Xu C, et al. Water steam modified crystallization and microstructure of mesoporous TiO2 nanofibers. *Ceram Int*. 2018;44(2):2158-2164. doi:10.1016/j.ceramint.2017.10.168

93. Vaiano V, Sannino D, Sacco O. Heterogeneous photocatalysis: how doping with nitrogen can improve the performance of semiconductor nanoparticles under visible light irradiation. In: *Nanomaterials for the Detection and Removal of Wastewater Pollutants*. Elsevier; 2020:285-301.

94. Lai Y, Sun L, Chen Y, Zhuang H, Lin C, Chin JW. Effects of the Structure of TiO[sub 2] Nanotube Array on Ti Substrate on Its Photocatalytic Activity. *J Electrochem Soc*. 2006;153(7):D123. doi:10.1149/1.2203112

95. Sauthier G, György E, Figueras A, Sánchez RS, Hernando J. Laser Synthesis and Characterization of Nitrogen-Doped TiO2 Vertically Aligned Columnar Array Photocatalysts. *J Phys Chem C*. 2012;116(27):14534-14540. doi:10.1021/jp304324e

96. Calisir MD, Gungor M, Demir A, Kilic A, Khan MM. Nitrogen-doped TiO2 fibers for visible-light-induced photocatalytic activities. *Ceram Int*. 2020;46(10):16743-16753.

97. Sathishkumar P, Pugazhenthiran N, Mangalaraja RV, Guesh K, Contreras D, Anandan S. Contemporary Achievements of Visible Light-Driven Nanocatalysts for the Environmental Applications. In: *Photocatalytic Functional Materials for Environmental Remediation*. John Wiley & Sons, Ltd; 2019:69-129. doi:https://doi.org/10.1002/9781119529941.ch3

98. Di Valentin C, Finazzi E, Pacchioni G, et al. N-doped TiO2: Theory and experiment. *Doping Funct Photoactive Semicond Met Oxides*. 2007;339(1):44-56. doi:10.1016/j.chemphys.2007.07.020

99. Liu D, Zhang M, Xie W, Sun L, Chen Y, Lei W. Porous BN/TiO2 hybrid nanosheets as highly efficient visible-light-driven photocatalysts. *Appl Catal B Environ*. 2017;207:72-78. doi:10.1016/j.apcatb.2017.02.011

100. Tran VA, Truong TT, Phan TAP, et al. Application of nitrogen-doped TiO2 nano-tubes in dye-sensitized solar cells. *Appl Surf Sci*. 2017;399:515-522. doi:10.1016/j.apsusc.2016.12.125

101. Shu T, Xiang P, Zhou ZM, et al. Mesoscopic nitrogen-doped TiO2 spheres for quantum dot-sensitized solar cells. *Electrochimica Acta*. 2012;68:166-171. doi:10.1016/j.electacta.2012.02.068

102. Garlisi C, Lai CY, George L, Chiesa M, Palmisano G. Relating Photoelectrochemistry and Wettability of Sputtered Cu- and N-Doped TiO2 Thin Films via an Integrated Approach. *J Phys Chem C*. 2018;122(23):12369-12376. doi:10.1021/acs.jpcc.8b03650

103. Le TXH, Charmette C, Bechelany M, Cretin M. Facile preparation of porous carbon cathode to eliminate paracetamol in aqueous medium using electro-Fenton system. *Electrochimica Acta*. 2016;188:378-384.

104. Li H, Zhang W, Pan W. Enhanced Photocatalytic Activity of Electrospun TiO2 Nanofibers with Optimal Anatase/Rutile Ratio. *J Am Ceram Soc*. 2011;94(10):3184-3187. doi:10.1111/j.1551-2916.2011.04748.x

105. Wang B, Leung MKH, Lu XY, Chen SY. Synthesis and photocatalytic activity of boron and fluorine codoped TiO2 nanosheets with reactive facets. *Appl Energy*. 2013;112:1190-1197. doi:10.1016/j.apenergy.2013.03.084

106. Film N, HaiyingWang, Hu Y. The Photocatalytic Property of Nitrogen-Doped TiO 2. In: ; 2015.

107. Wang H, Hu Y. The Photocatalytic Property of Nitrogen-Doped TiO2 Nanoball Film. *Int J Photoenergy*. 2013;2013:1-6.

108. Li X, Liu P, Mao Y, Xing M, Zhang J. Preparation of homogeneous nitrogen-doped mesoporous TiO2 spheres with enhanced visible-light photocatalysis. *Appl Catal B Environ*. 2015;164:352-359. doi:10.1016/j.apcatb.2014.09.053

109. Bakar SA, Ribeiro C. Nitrogen-doped titanium dioxide: An overview of material design and dimensionality effect over modern applications. *J Photochem Photobiol C Photochem Rev*. 2016;27:1-29. doi:10.1016/j.jphotochemrev.2016.05.001

110. Choi WH, Lee CH, Kim H eun, Lee SU, Bang JH. Designing a high-performance nitrogen-doped titanium dioxide anode material for lithium-ion batteries by unravelling the nitrogen doping effect. *Nano Energy*. 2020;74:104829. doi:10.1016/j.nanoen.2020.104829

111. Noorisepehr M, Kakavandi B, Isari AA, et al. Sulfate radical-based oxidative degradation of acetaminophen over an efficient hybrid system: Peroxydisulfate decomposed by ferroferric oxide nanocatalyst anchored on activated carbon and UV light. *Sep Purif Technol*. 2020;250:116950. doi:10.1016/j.seppur.2020.116950

112. Dirany A, Sirés I, Oturan N, Özcan A, Oturan MA. Electrochemical treatment of the antibiotic sulfachloropyridazine: kinetics, reaction pathways, and toxicity evolution. *Environ Sci Technol*. 2012;46(7):4074-4082.

113. Le TXH, Nguyen TV, Yacouba ZA, et al. Correlation between degradation pathway and toxicity of acetaminophen and its by-products by using the electro-Fenton process in aqueous media. *Chemosphere*. 2017;172:1-9. doi:https://doi.org/10.1016/j.chemosphere.2016.12.060

114. Zhang J, Sun B, Xiong X, et al. Removal of emerging pollutants by Ru/TiO2-catalyzed permanganate oxidation. *Water Res*. 2014;63:262-270. doi:10.1016/j.watres.2014.06.028

115. Zhao B, Yu H, Liu Y, et al. Enhanced photoelectrocatalytic degradation of acetaminophen using a bifacial electrode of praseodymium-polyethylene glycol-PbO2//Ti//TiO2-nanotubes. *Chem Eng J*. 2021;410:128337. doi:10.1016/j.cej.2020.128337

116. Yang L, Yu LE, Ray MB. Photocatalytic Oxidation of Paracetamol: Dominant Reactants, Intermediates, and Reaction Mechanisms. *Environ Sci Technol*. 2009;43(2):460-465. doi:10.1021/es8020099

117. Le TXH, Nguyen TV, Yacouba ZA, et al. Toxicity removal assessments related to degradation pathways of azo dyes: Toward an optimization of Electro-Fenton treatment. *Chemosphere*. 2016;161:308-318. doi:10.1016/j.chemosphere.2016.06.108